



Tobias Kinner-Becker, Matthias Hettig, Jens Sölter, and Daniel Meyer

Analysis of internal material loads and Process Signature Components in deep rolling

Journal Article as: peer-reviewed accepted version (Postprint)

DOI of this document* (secondary publication): 10.26092/elib/2407

Publication date of this document: 25/08/2023

* for better findability or for reliable citation

Recommended Citation (primary publication/Version of Record) incl. DOI:

Tobias Kinner-Becker, Matthias Hettig, Jens Sölter, Daniel Meyer,
Analysis of internal material loads and Process Signature Components in deep rolling,
CIRP Journal of Manufacturing Science and Technology, Volume 35, 2021, Pages 400-409, ISSN 1755-5817,
<https://doi.org/10.1016/j.cirpj.2021.06.024>.

Please note that the version of this document may differ from the final published version (Version of Record/primary publication) in terms of copy-editing, pagination, publication date and DOI. Please cite the version that you actually used. Before citing, you are also advised to check the publisher's website for any subsequent corrections or retractions (see also <https://retractionwatch.com/>).

This document is made available under a Creative Commons licence.

The license information is available online: <https://creativecommons.org/licenses/by-nc-nd/4.0/>

Take down policy

If you believe that this document or any material on this site infringes copyright, please contact publizieren@suub.uni-bremen.de with full details and we will remove access to the material.

Analysis of internal material loads and Process Signature Components in deep rolling

Tobias Kinner-Becker^{a,b}, Matthias Hettig^{a,b}, Jens Sölter^{a,b}, and Daniel Meyer^{a,b}

^a University of Bremen, MAPEX Center for Materials and Processes, Faculty of Production Engineering, Research Group for Manufacturing Processes, Bremen, Germany

^b Leibniz Institute for Materials Engineering, Department of Manufacturing Technologies, Badgasteiner Str.3, D-28359 Bremen, Germany

1. Abstract

The high mechanical loads in deep rolling lead to a beneficial surface topography, hardness alterations, and compressive residual stresses. The generation of defined residual stress values has been achieved in a mainly iterative way, as the relevant internal material loads occurring during the process could not be considered. They are difficult to determine experimentally and well-validated models are required to deduce them e.g. from finite element (FE) simulations. In this study, a 3D FE model has been developed to analyze the strains in the workpiece material as a measure for the internal material load during the process. The residual stress profiles were measured by x-ray-diffraction and are presented in a way that allows for deriving the internal material loads required to induce a desired residual stress state.

Keywords: Finite element method (FEM), Simulation, Surface modification, Deep rolling, Process Signature, Residual stress

2. Introduction

Mechanical surface treatment by processes such as machine hammer peening [1], burnishing [2,3], and deep rolling [4] are widely applied to generate beneficial surface and subsurface characteristics. The high relevance of advantageous surface integrity has been pointed out e.g. by Jawahir et al. [5] and Schulze et al. [6] for material removal processes as well as mechanical surface treatments. Due to the potential to create near-optical surface topography, hardness alterations based on strain hardening and high compressive residual stresses at high depths, the deep rolling process was introduced to a wide range of industrial applications. As the mechanical load of a deep rolling process can be described by process variables such as the deep rolling force F_r or the deep rolling pressure p_r of hydrostatically supported tools, many publications focus on these parameters regarding the resulting surface layer modification such as reduced roughness, hardness alterations or induced residual stresses [7, 8, 9]. From these results, it can be concluded that the validity of identified correlations is always limited to a certain range of those parameters. The explanation for this observation can be inferred from Brinksmeier et al. [10], who emphasize the relevance of considering internal material loads occurring within the material during the process. Process quantities such as forces and pressure (mechanical load) and the heat flux in the contact zone (thermal load) act as external material loads on the workpiece boundary and propagate in the material as time-dependent temperature and strain fields representing the internal material loads during the manufacturing process. It is supposed that the material responds to these quantities as they describe the

physical cause of the material modifications rather than the process quantities. However, there was no adequate description of the internal material loads in deep rolling, preventing a systematic and mechanism-oriented analysis of the interrelations leading to a certain surface modification. Prior work has been focused on analytically calculated equivalent stresses based on the Hertzian equations [11]. Furthermore, only the results from deep rolling single tracks once [11] or up to three times [12] without any lateral offset (feed) were considered in the past due to the lack of validated numerical models allowing for consideration of the effects occurring when an area is deep rolled. In industrial practice, the kinematics of deep rolling processes are characterized by a certain rolling velocity v_{dr} and the feed f_{dr} (for cylindrical workpieces), respectively the track offset f_o (for prismatic workpieces). First indications for the relevance of the lateral offset (feed or track offset) were revealed by Kinner-Becker et al. [13] showing that the residual stresses after deep rolling several tracks consecutively with a certain feed develops with each additional track being deep rolled. Consequently, the work presented here aims at identifying and quantifying the relevant internal material loads in a deep rolling process characterized by generating a strain-hardened area. The internal material loads are then to be correlated with experimental and numerical data to derive so-called Process Signature Components as introduced by Brinksmeier et al. [14]. Process Signature Components are discussed [15] to carry the potential to predict the resulting surface and subsurface characteristics in a knowledge-based way rather than optimizing a process iteratively. The results enable the computation of suitable internal material loads for a given, desired residual stress depth profile (solution of the inverse problem in manufacturing).

3. Approach and procedure

As the experimental analysis of mechanically induced internal material loads is very challenging and yet no suitable method is available, a model-based approach to determine these quantities has been chosen. A 3D finite element (FE) model has been developed and validated based on a comparison of the resulting residual stress depth profiles with experimental data (see 4.2). In the experiments and the simulations, multiple contacts including the tool's feed have been taken into account. Deep rolling experiments have been performed at different mechanical loads applying different feeds to account for a wide range of combinations affecting the internal material loads (4.1). The resulting material modifications by means of residual stress depth profiles have been compared (5.1). The good agreement between experimental and numerical data allowed for the identification and quantification of the relevant internal material loads (5.2). Those were subsequently used to establish Process Signature Components (5.2). An approach is presented to use the obtained Process Signature Components to inversely determine the necessary rolling pressure from a wanted residual stress state (6). The overall approach is summarized in Figure 1.

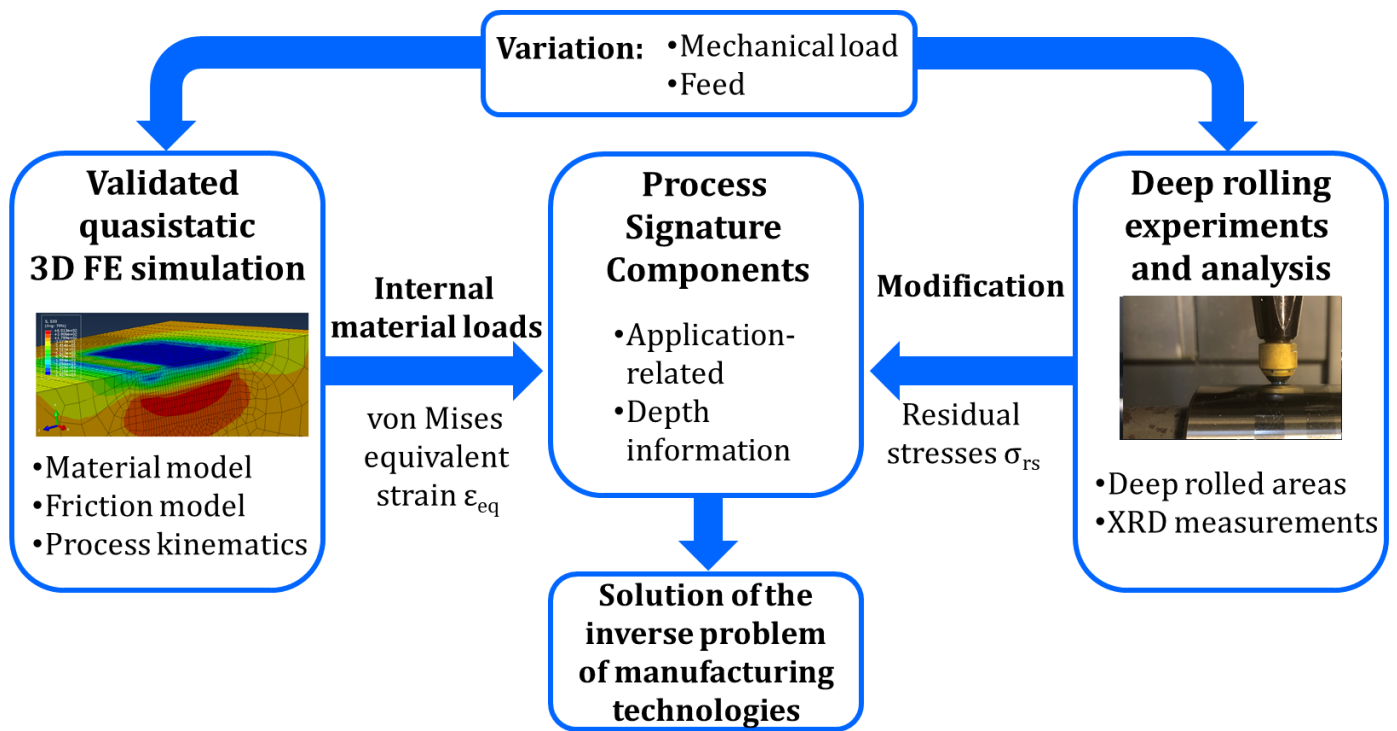


Figure 1 - Approach for the analysis of the interrelations between internal material loads and surface modifications in deep rolling

4. Experimental and simulative setup and design

4.1. Deep rolling experiments

Deep rolling experiments were conducted using pre-ground cylindrical specimens (length 140 mm, \varnothing 58 mm) made of AISI 4140 (42CrMo4) quenched and tempered to 47 HRC hardness. The pre-grinding step was done to correct form deviations after the heat treatment and to remove the present oxide layer. All experiments were performed on a conventional CNC Lathe (DMG Mori Seiki NEF 400) and carried out threefold for each combination of deep rolling parameters. A hydrostatically supported deep rolling tool with a sphere diameter of $d_b = 6$ mm (Ecoroll HG6) was applied. The deep rolling force F_r was generated using an external hydraulic unit. The pressure was transferred to the deep rolling tool using an 8 % metalworking fluid emulsion (Rhenus TS 440). The tools are equipped with a lift and are self-adjusting to compensate for clamping errors or form deviations. Due to this self-adjusting mechanism, a constant force is applied to the whole workpiece during the process. Regarding the process parameters, the circumferential velocity of the workpiece was kept constant at $v_{dr} = 7.29$ m/min. This is different to industrial deep rolling processes with circumferential velocities of around 100 m/min. The relatively low deep rolling velocity was chosen to facilitate the comparability with the results of the FE simulations.

Due to the resulting comparatively low strain rates, strain rate hardening could be neglected, as according to Emde, quenched and tempered AISI 4140 shows no strain rate hardening below a strain rate of approximately 10 /s and for total achieved strains below approximately 15 % [16]. Quasistatic tensile tests could therefore be

utilized for parameterizing the material model. However, previous researchers described a very limited effect of varying deep rolling velocities on the resulting surface and subsurface characteristics [17]. The deep rolling force and deep rolling feed f_{dr} were varied as indicated in Figure 2. On each specimen, four deep rolled areas were generated. Each area was 10 mm wide in axial direction with 8 mm of unprocessed material between them to exclude interactions between the manufactured areas. During the process, the forces were measured using a 3-axis dynamometer mounted between the tool holder and the lathe. The measured forces (also listed in figure 2) were averaged and the mean values later used as input parameters for the numerical simulations (4.2). Resulting residual stresses parallel ($\sigma_{rs||}$) and perpendicular ($\sigma_{rs\perp}$) to the deep rolling direction were measured by X-ray diffraction applying the $\sin^2\text{-}\Psi$ -method using a 5-circle θ - 2θ XRD device (Seifert XRD MZ VI E) with a chromium anode and an aperture of 2 mm. The X-ray spot was located at the center of the deep rolled areas.

To allow for a systematic analysis of the effects of the mechanical load, the applied deep rolling force F_r was specifically varied on three levels. The force levels were chosen to match the process forces used in previous hertzian based load-oriented investigations by Meyer & Kämmler [11], where the rolling forces were analytically derived from certain levels of hertzian contact stresses to be achieved (2250, 3250 and 4500 MPa) . The feed was varied on two levels in the experiments. Two additional feeds were taken into account in the simulations ($f_{dr} = 0.2, 0.4$ mm). The process forces and parameters for all experiments and the experimental setup are shown in Figure 2. The chemical and mechanical properties of the workpiece material are listed in Table 1.

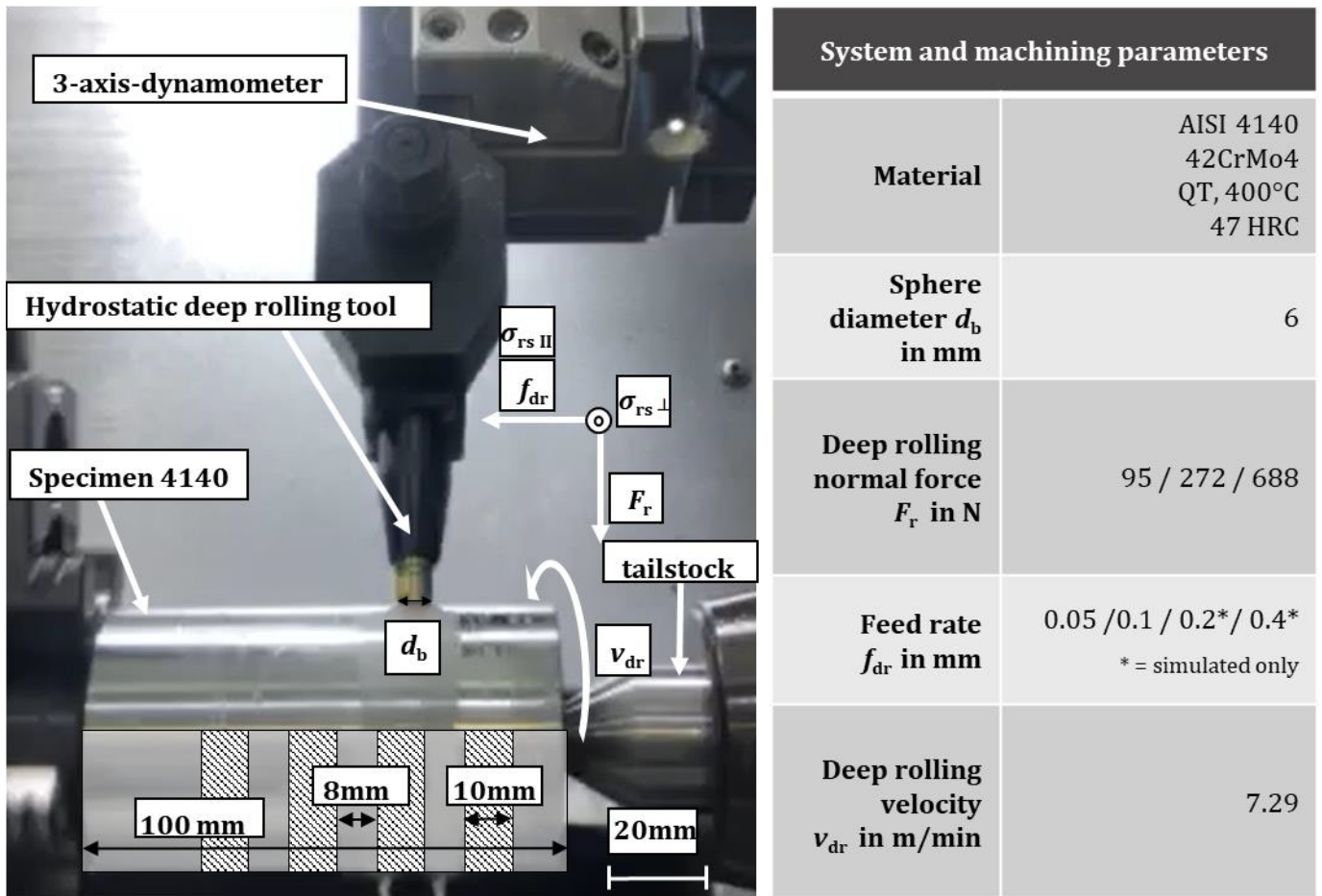


Figure 2 - Experimental setup and system and machining parameters

Chemical properties							
Element	C	Si	Mn	P	S	Cr	Mo
%	0.43	0.26	0.74	0.010	< 0.001	1.09	0.25
Mechanical properties (at 20 °C)							
Property	Elastic limit	Ultimate strength	Young's Modulus	Poisson ratio	Density	Hardness	
Value	1435 MPa	1625 MPa	206.5 GPa	0.274	7830 kg/m ²	47 HRC	

Table 1 - Chemical and mechanical properties of the used AISI 4140 (42CrMo4)

4.2. 3D Finite Element simulation

The deep rolling process was modeled using the FE software Simulia Abaqus 2020. As deep rolling can be considered as a quasi-static process (apart from the initial indentation), an implicit procedure was used. The whole process consists of two separate models analyzing i) the deep rolling process itself and ii) a springback analysis to obtain the equilibrium state of the workpiece after unclamping. The simulation of the process consists of three steps in total. First, a displacement-controlled indentation with an indentation depth of 5 μm was modeled in a static implicit step to achieve a fast convergence of the contact establishment between tool and workpiece. Then, in another static implicit step, a load-controlled indentation takes place until the average rolling force F_r measured in the experiments is reached. A dynamic implicit step finally models the deep rolling

of a single track by moving the tool linearly along the surface. To model processing of the whole surface, the final material state after each track acts as input to the simulation of the subsequent track. All simulation steps are purely mechanical analyses, as the heat generation in deep rolling using a freely rotating hydrostatically supported tool (metalworking fluid) is negligible. A fully coupled simulation was performed to verify this assumption and showed a temperature increase of 2.5 °C (from 20 °C) in the workpiece during deep rolling. In the simulation a deep rolling force of $F_r = 726$ N, an isotropic friction coefficient of 0.05, an inelastic heat fraction of 90 % and 100 % of the generated friction heat dissipating into the workpiece were chosen. Heat convection due to the metalworking fluid was neglected.

4.2.1. Geometry and Boundary conditions

As the computational effort for a single track is high and a large variation of process parameters had to be simulated, the number of tracks per surface processing had to be restricted. It was found that for the highest load, processing a workpiece material of 2 mm in feed direction and 6 mm in rolling direction, is sufficient to obtain a homogeneously modified zone in the middle of the deep rolled area (as illustrated for $\sigma_{rs\perp}$ in Figure 3c). This results in the simulation of 30 tracks for a feed of $f_{dr} = 0.05$ mm, 15 tracks for $f_{dr} = 0.1$ mm, 8 tracks for $f_{dr} = 0.2$ mm, and 5 tracks for $f_{dr} = 0.4$ mm. The total workpiece length and width were dimensioned to 10 mm, respectively 6.6 mm. This allows for unprocessed workpiece material between the part boundaries and the processed area so that the simulation results are not influenced by the boundaries. The height difference in a path length of 10 mm on a cylinder with $R = 58$ mm amounts to 0.43 mm due to the curvature of the workpiece of 0.0345 °/mm. It is assumed that this can be neglected regarding the influence on residual stress distributions. The model geometry can be seen in Figure 3a. The modeled workpiece is divided into a fine section, where the processing takes place and a coarse section for the surrounding material (shown in figure 3b). In the fine section, the element dimensions are fixed in y- and x-direction at 50 μm and 150 μm respectively. The element size in z-direction gradually increases from 35 μm to 150 μm . The element dimensions in the coarse section are graded up to 1 mm at the boundaries. In total, this results in 51,255 C3D8 elements. During deep rolling, all nodes at the bottom surface are fixed in every degree of freedom (dof). For the springback analysis, only the bottom corner nodes are kept fixed, as indicated in Figure 3a.

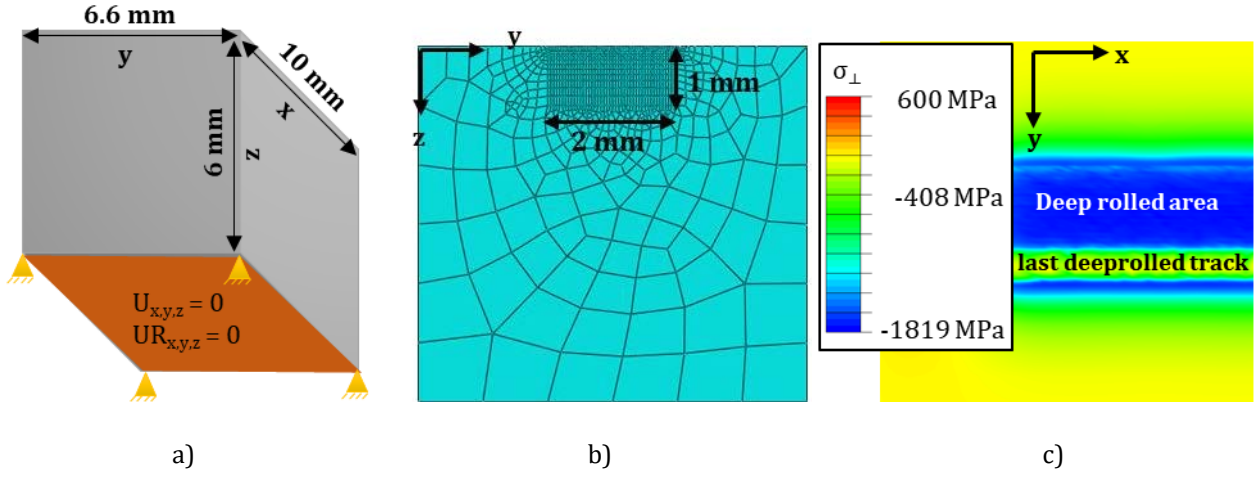


Figure 3 - a) Dimensions of the modeled workpiece. Boundary conditions during deep rolling (orange) and during springback (yellow), b) Simulation mesh in the front view, c) Residual stresses in deep rolling direction at the surface after deep rolling of 15 tracks with $F_r = 688 \text{ N}$.

4.2.2. Material model and initial validation

The plastic and elastic material parameters were derived from an uniaxial tensile test at a strain rate of 0.1/s. The basic material parameters are already listed in table 1. The full stress-strain curve of the uniaxial tensile test, can be seen in Figure 4. To validate the model setup, residual stress depth profiles were compared between simulation and experiment for the deep rolling of prismatic workpieces. For this purpose, slightly different parameters from the main test series were deliberately chosen. It was found that a kinematic strain hardening model leads to a better prediction of the maximum compressive residual stress than an isotropic hardening model. A non-linear kinematic hardening model [18] with three backstresses was therefore used to model the strain hardening of the material. In this model, the center of the yield surface, respectively the total back stress tensor is calculated from the single back stress components as:

$$\alpha = \sum_i \alpha_i \quad (1)$$

where the evolution of the back stress components is defined as:

$$\dot{\alpha}_i = C_k \frac{1}{\sigma_y} (\sigma - \alpha) \dot{\epsilon}_{pl,acc} - \gamma_k \alpha_k \dot{\epsilon}_{pl,acc} \quad (2)$$

where C_k and γ_k are the model parameters that need to be determined, $\epsilon_{pl,acc}$ is the accumulated plastic strain and σ_y the size of the yield surface. In the experiments, tangential process forces had been measured which indicate friction between tool and workpiece. Taking friction into account in the simulation was found beneficial regarding the agreement between simulation and experiment. Isotropic Coulomb friction between tool and workpiece was assumed. By analyzing the process forces during the experiments, an average friction coefficient of 0.03 has been determined. The tool was modelled as an analytical rigid body since the elastic modulus of the ceramic tool material is much higher than that of the workpiece material. The comparison of the residual stress

in rolling direction is shown in Figure 5 for one of the used validation cases with the optimized model. As can be seen, the simulated residual stress depth profile follows the measured values qualitatively well. Quantitatively the simulated residual stresses are overestimated.

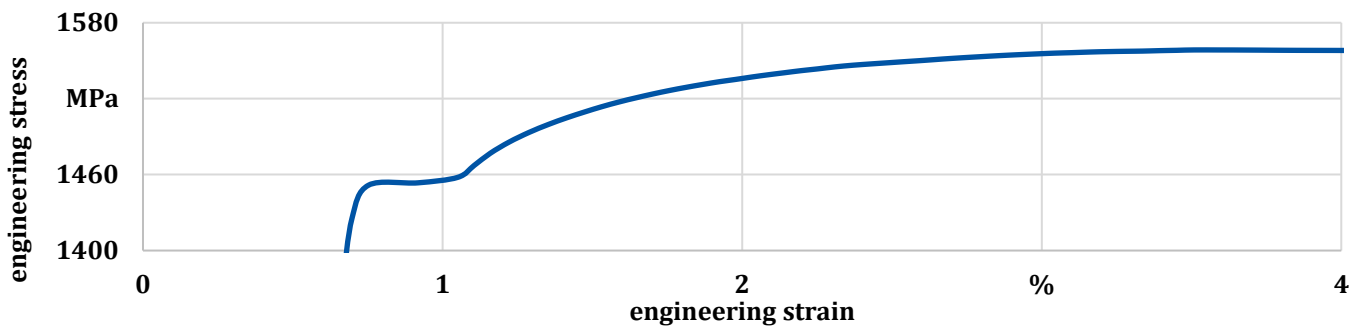


Figure 4 – Stress-strain curve of tensile testing with a strain rate of 0.1/s.

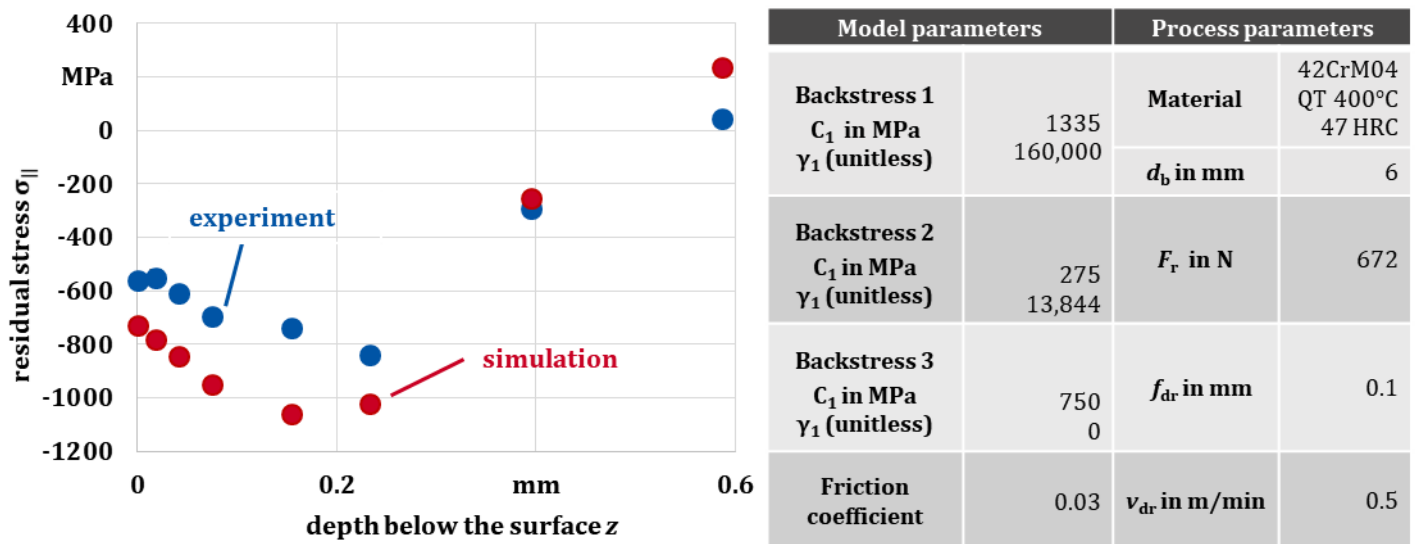


Figure 5 – Left: Comparison of $\sigma_{||}$ after deep rolling a prismatic workpiece with a rolling force of $F_r = 672$ N. Right: Model and process parameters.

5. Results

5.1. Comparison between simulated and experimental residual stress depth profiles

Experiments have shown that deep rolling of quenched and tempered AISI4140 does not lead to significant hardness alterations [19]. Thus, the main investigations focussed on residual stresses. Both the experimentally measured and the numerically calculated residual stress depth profiles show the typical behavior after deep rolling (Figure 6). High compressive residual stresses at the surface are accompanied by maximum compressive residual stresses in rolling direction below the surface. At higher deep rolling forces, the location of the maximum compressive residual stresses perpendicular to the rolling direction shift to lower depths and is to be found at the surface for the highest deep rolling force. The good qualitative agreement of the experimental and numerically assessed residual stress depth profiles reveals quantitative deviations which increase at higher

forces. Generally, the simulation overestimates the compressive residual stresses. Two main reasons are assumed to be responsible for this observation. Firstly, the used material model has a big influence on the simulated residual stresses. As data taken from single tensile tests cannot account for the Bauschinger effect, model parameters derived from cyclic tension-compression tests will instead be used in the future. The second reason is the rather coarse mesh resolution. A finer mesh leads to a better agreement between experiment and simulation at the surface, but would not be feasible to implement due to the computational cost for the necessary high number of simulated tracks. Depending on the deep rolling force, the depth effect of the process varies from less than 200 μm to ca. 500 μm . Simulated residual stresses agree qualitatively well with the measurements. The predictive power of the model established in section 4 is thereby reconfirmed. This is of high relevance for the next step (5.2) which aimed at the identification and quantification of the internal material loads. Process Signature Components were then derived by correlating the residual stresses with the internal material loads (5.3).

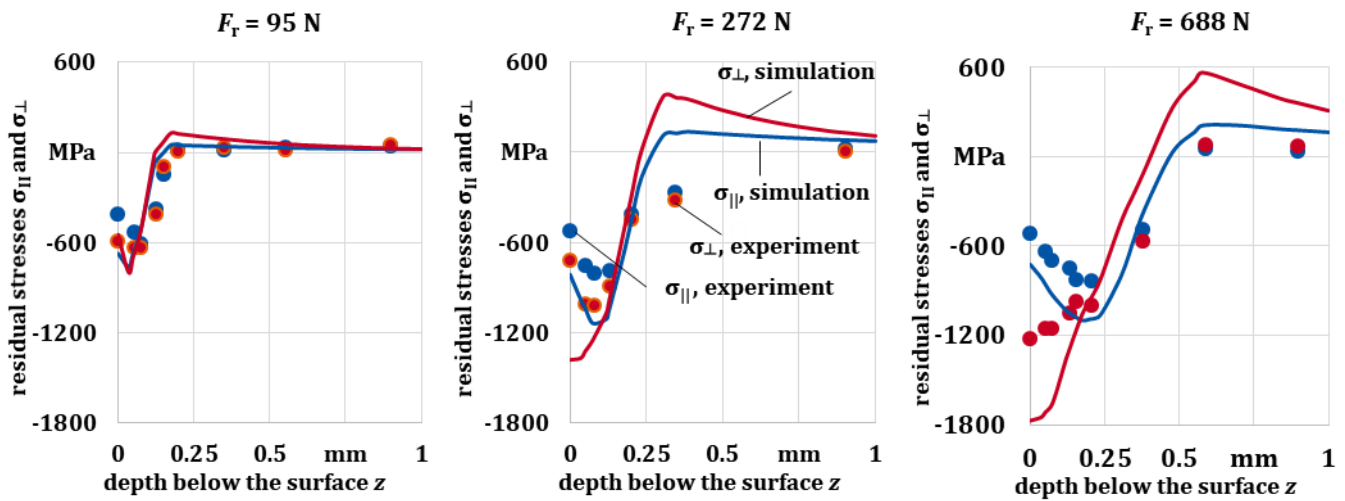


Figure 6 - Simulated and experimental residual stress depth profiles ($d_b = 6 \text{ mm}$, $v_{dr} = 7.29 \text{ mm/min}$, $f_{dr} = 0.1 \text{ mm}$).

5.2. Identification and quantification of the internal material loads

A very specific challenge of the numerical analysis of the internal material loads during deep rolling is to understand when and how to deduce them from the model. Thus, the development of the stress and strain fields below the deep rolling tool during the process were carefully investigated in a cylindrical area around the tool center during processing. This was repeated for every simulated track when the tool had passed half the track length as shown schematically in Figure 7.

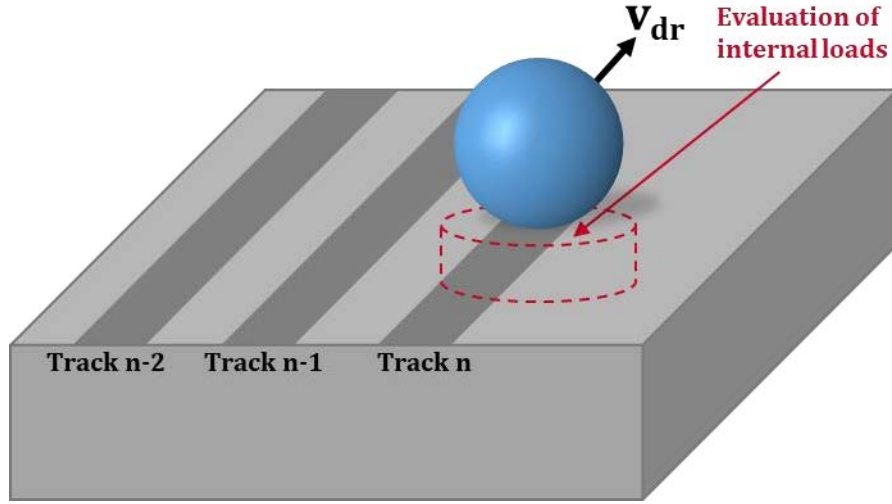


Figure 7 - Analysis of the internal material loads during deep rolling subsequent tracks.

For the approach presented in Figure 7, different quantities were considered to be relevant for the material's response during deep rolling. Taking into account the mechanism of strain hardening, which is based on plastic deformation, strain-related quantities were the most promising. And indeed, in an iterative procedure, the (von Mises) equivalent strain ε_{eq} was confirmed to be suitable. The equivalent strain ε_{eq} was calculated from the (true) strain tensor components according to equation (3).

$$\varepsilon_{eq} = \sqrt{\varepsilon_x^2 + \varepsilon_y^2 + \varepsilon_z^2 - \varepsilon_x \varepsilon_y - \varepsilon_x \varepsilon_z - \varepsilon_y \varepsilon_z + 3(\varepsilon_{xy}^2 + \varepsilon_{xz}^2 + \varepsilon_{yz}^2)}. \quad (3)$$

In the cylindrical region indicated in Figure 7, the maximum value $\varepsilon_{eq,max}$ of the equivalent strain was determined and used as internal material load. The depth profile of ε_{eq} at this position was determined as well (see Figure 10b).

For different levels of the mechanical loads, i.e. deep rolling forces, Figure 8 depicts the development of the maximum internal material load below the tool for a constant feed of $f_{dr} = 0.1$ mm. Independently from the deep rolling force, a constant level of the maximum equivalent strain is achieved after a total feed $f_{dr,total}$ of 1 mm (and before for $F_r = 272$ N and $F_r = 95$ N). The obtained maximum ε_{eq} is 0.34 for the highest deep rolling force of $F_r = 688$ N, $\varepsilon_{eq} = 0.10$ for a deep rolling force of $F_r = 272$ N, and $\varepsilon_{eq} = 0.02$ for the lowest deep rolling force of $F_r = 95$ N.

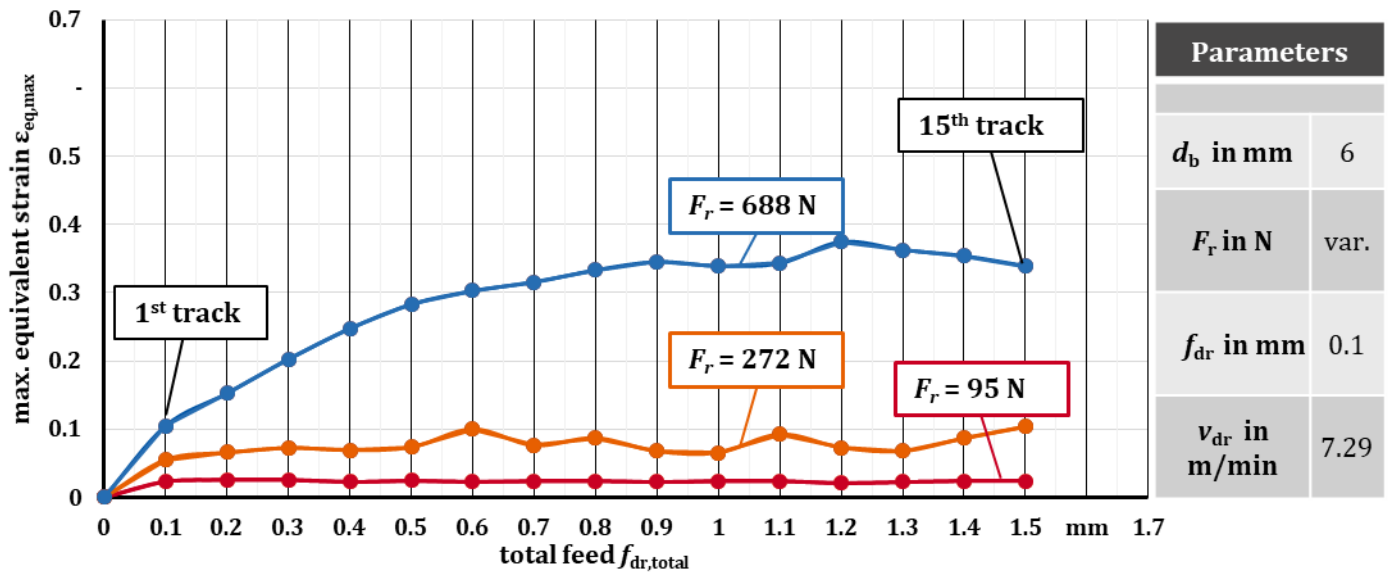


Figure 8 - Dependence of the maximum equivalent strain $\epsilon_{eq,max}$ below the tool on the width of the manufactured area (number of deep rolled tracks) for varied deep rolling forces

Figure 9 shows the development of the maximum equivalent strain $\epsilon_{eq,max}$ below the deep rolling tool when moving along the workpiece for each track with a feed of 0.05 mm, 0.1 mm, 0.2 mm, and 0.4 mm at a deep rolling force of $F_r = 688$ N. A constant level of the maximum internal material load below the tool is achieved for all feeds after a total feed of 1 mm. It can be seen that the internal material load depends on the feed and increases with decreasing feed. This is not surprising, as the chosen internal material load variable is a strain measure. The equivalent strain in track n is affected by the strains generated during deep rolling of preceding tracks $n-1$, $n-2$, etc. The number of previously deep rolled tracks that could affect the strain distribution in track n increases with decreasing feed and therefore increases the measured internal material load during deep rolling track n too.

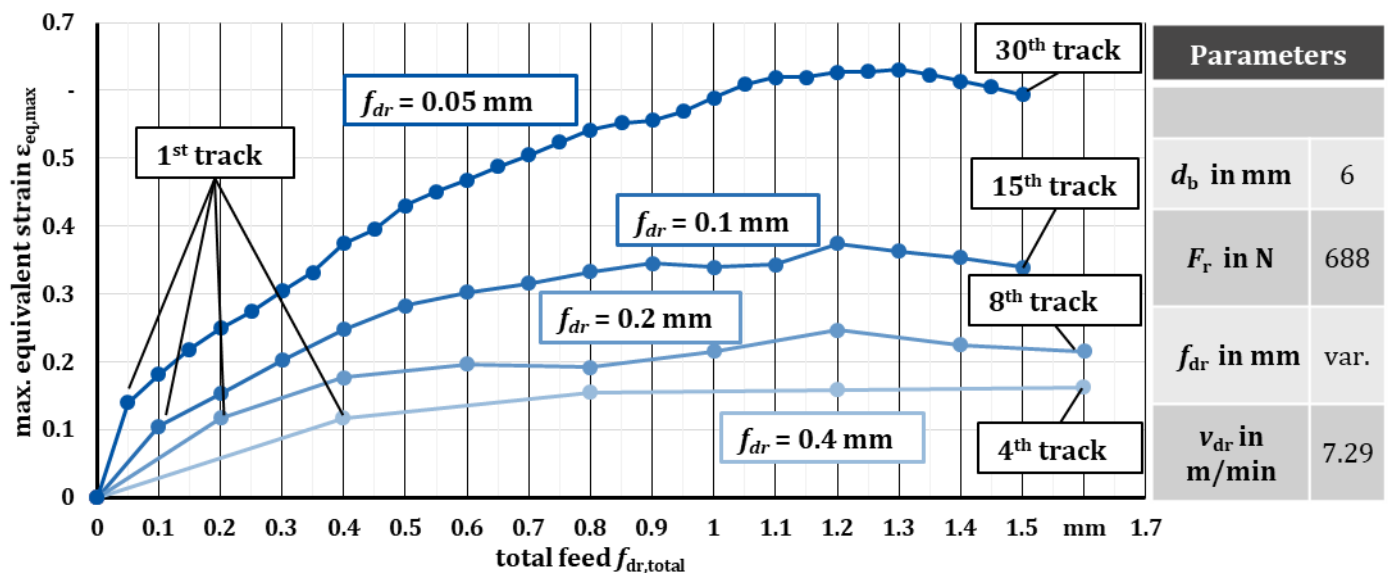


Figure 9 - Development of the maximum equivalent strain $\epsilon_{eq,max}$ below the deep rolling tool along with the movement in feed direction at varied feeds and a deep rolling force of 688 N.

In the following, Process Signature Components will be derived which correlate the maximum values of the residual stress with the maximum internal material load during processing. However, the maximum internal material load and the maximum compressive residual stresses appear in different depths depending on the chosen mechanical load (see Figure 6, respectively Figure 10). As the present work allows to deduce Process Signature Components based on validated data from an elastoplastic model, a depth-resolved analysis of the interrelation between internal material loads and material modifications will be performed additionally. Figure 10 shows the used depth profiles of the internal material load ϵ_{eq} below the tool during deep rolling for all three deep rolling forces at a feed of 0.1 mm. The location of the maximum internal material load moves closer to the surface with lower deep rolling forces, which is in good agreement with the movement of the maximum compressive stresses deeper into the material at higher deep rolling forces (Figure 6).

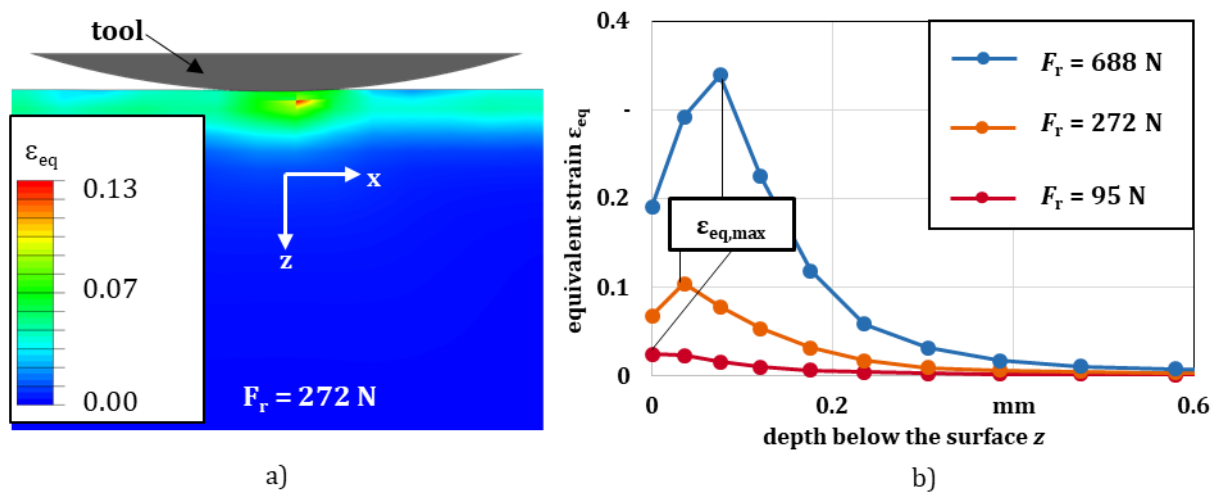


Figure 10 – Simulated equivalent strain distribution below the deep rolling tool (a) and simulated depth profiles (b) of the internal material load after a constant strain field below the deep rolling tool is reached (here: after a total feed $f_{dr,total} = 1 \text{ mm}$)

5.3. Process Signature Components for deep rolling

According to Brinksmeier et al and Grzesik [14, 15], Process Signature Components represent the interrelation between the internal material loads and the material modification as a material's response to the loads of a manufacturing process. The majority of publications is dealing with Process Signature Components for processes with a dominant mechanical impact such as deep rolling discuss the (analytically assessed) maximum internal material load based on equivalent stresses and the resulting maximum compressive residual stresses. The gained data from FE simulations (5.2) and experiments (5.1) allows to establish these correlations to be based on the elastoplastically assessed strains ϵ_{eq} as the characteristic quantity for the internal material loads. Figure 11 correlates the determined maximum internal material loads with the experimentally and numerically assessed maximum compressive residual stresses for a feed of $f_{dr} = 0.1 \text{ mm}$. Both the maximum compressive residual stresses parallel and perpendicular to the rolling direction are given.

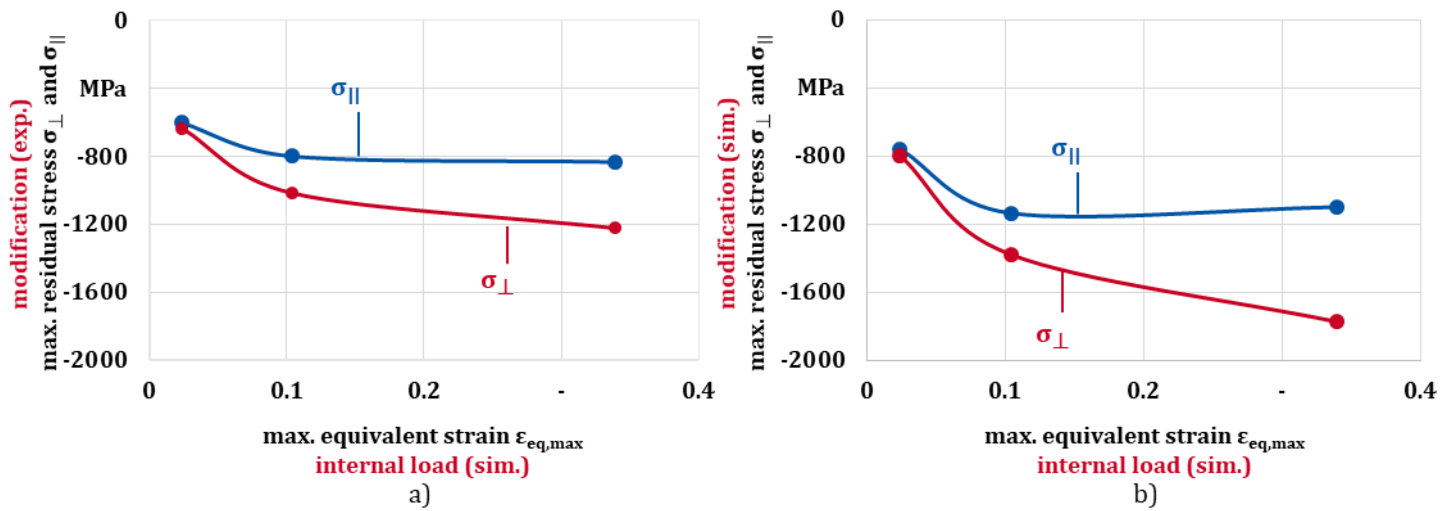


Figure 11 – Process Signature Components for deep rolled surfaces considering the maximum internal material loads and the maximum material modification at a feed of $f_{dr} = 0.1$ mm with experimental residual stresses (a) and simulated residual stresses (b).

To get an idea of a potential influence of the feed on the Process Signature Components, Figure 12 summarizes the numerically assessed Process Signature components based on maximum values for different feeds. As can be seen, they follow the same general trend, apart from some outliers. The maximum equivalent strain is therefore a good indicator for the achieved maximum residual stress regardless of the chosen feed, which emphasizes its suitability as a measure for the internal material load in deep rolling.

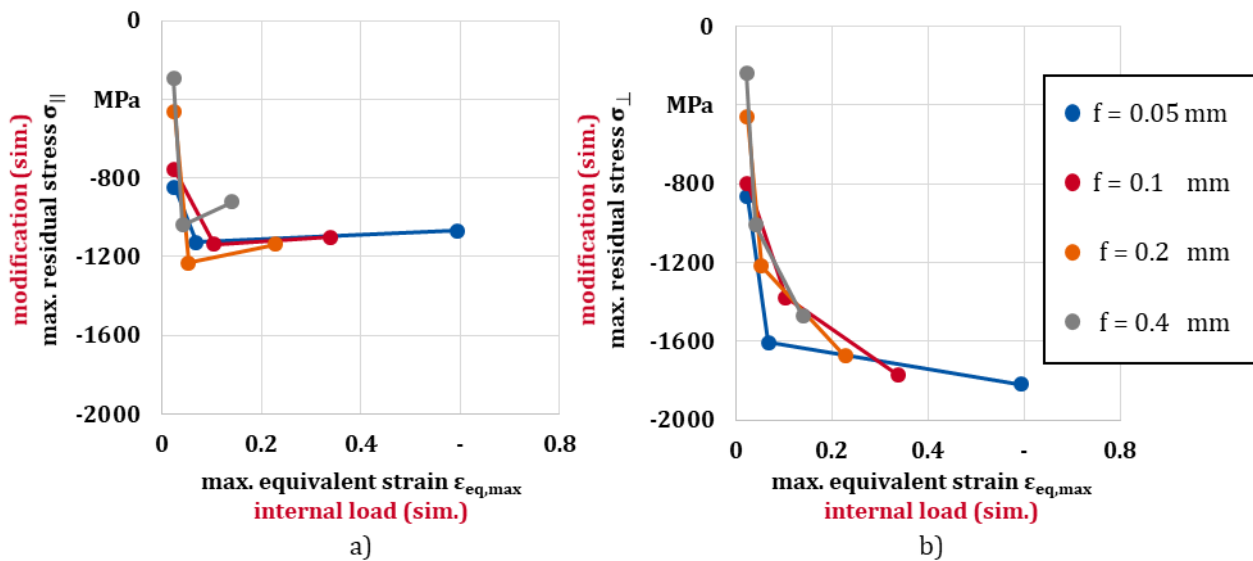


Figure 12 – Process Signature Components for deep rolled surfaces considering the maximum internal material loads and the maximum material modification at varied feeds for residual stresses in rolling direction (a) and residual stresses in feed direction (b).

While the maximum values $\epsilon_{eq,max}$ were used for the Process Signature Components shown in Figures 11 and 12, the depth profiles shown in Figure 10 also allow the use of the internal material loads ϵ_{eq} at defined depths to generate depth-resolved Process Signature Components. Those are essential to predict the resulting surface and subsurface properties. The correlations of maximum values does not allow to derive suitable process parameters

to achieve a desired level of residual stresses at the surface or in a given depth. Figure 13 presents Process Signature Components indicating the correlation between the internal material load in a certain depth and the resulting residual stresses in that same depth for the experimental (13a) and numerical (13b) data. Both graphs show a comparable and plausible course. Independent from the depth, higher internal material loads lead to higher compressive residual stresses. Interestingly, there are certain parts of the correlations indicating that the material's response to a certain internal material load changes when looking at different depths. This highlights that for residual stress depth profiles, the residual stress is an integral quantity and is therefore influenced by the complete strain depth profile. This emphasizes the value of depth-resolved Process Signatures.

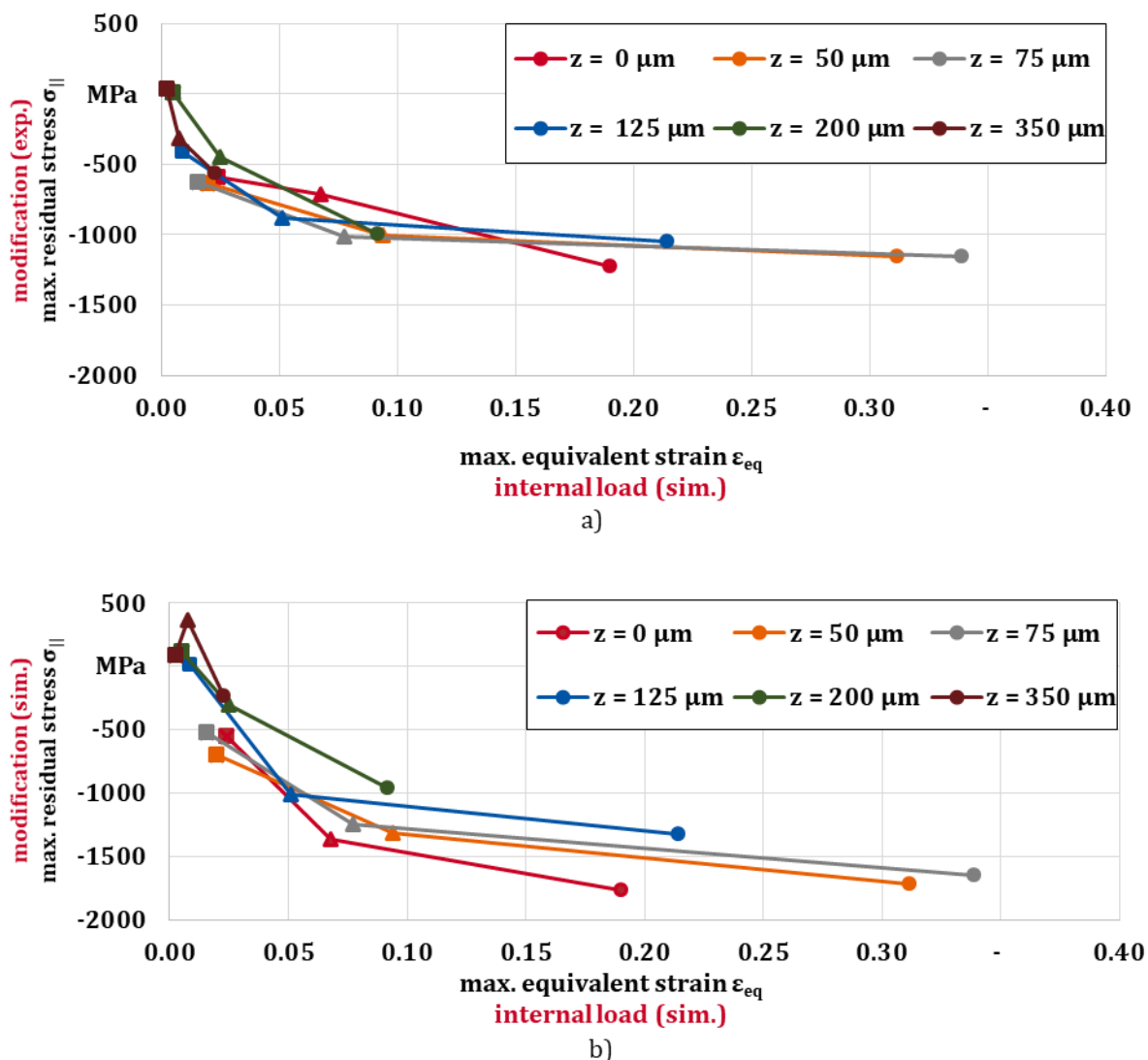


Figure 13- Depth-resolved Process Signature Components correlating the internal material load $\epsilon_{eq,max}$ in a certain depth to experimentally (a) and simulated (b) residual stresses

6. Conclusions

Deep rolling is a well-established process to induce beneficial surface and subsurface characteristics. Jawahir and colleagues [5] presented the results of an international round robin test aiming at inducing a given residual

stress state at the surface of steel samples by a process and parameters of choice. Without optimizing the process iteratively, most samples showed large deviations from the target value. This strongly confirmed the need for systematic approaches to allow “first-time-right” manufacturing. The goal of this paper was to close the knowledge gap with respect to the internal material loads during deep rolling. A validated 3D FE-simulation was used to identify and quantify the relevant strains during deep rolling. The good agreement between experimental and numerical data allows a better understanding of the process and the material’s response. The depth-resolved Process Signature components enable to inversely determine the necessary process parameters to choose for a desired residual stress at a specific depth. The use of the knowledge gained is demonstrated in Figure 14. Using the depth-resolved Process Signature Component (14b) and defining a desired residual stress level of -900 MPa at the surface ($z = 0 \mu\text{m}$) after deep rolling, a required internal material load of $\varepsilon_{\text{eq,max}} = 0.113$ can be deduced (green dotted lines). The data from the FE-simulation allows to correlate the internal material loads with the experimentally measured deep rolling force (14d). By interpolation, a deep rolling force of $F_r = 430 \text{ N}$ is identified to be necessary. The deep rolling force is a direct result of a comparably simple equation where the deep rolling pressure set on the pump and the diameter of the tool are the only relevant factors:

$$F_r = (p_r \cdot (0.5 + d_b)^2 \cdot \pi) / 10 \quad (2)$$

As demonstrated in Figure 14c, a pressure of 152 bar will result in a deep rolling force of 430 N. As all steps of this causal sequence are known and the correlations allow an interpolation, in this example, it would be possible to provide the desired information. Deep rolling with a tool diameter of 6 mm and a deep rolling pressure of 152 bar should result in -900 MPa compressive residual stresses at the surface. This comparably simple example stresses the potential of the concept of Process Signatures as proposed by Brinksmeier et al [10].

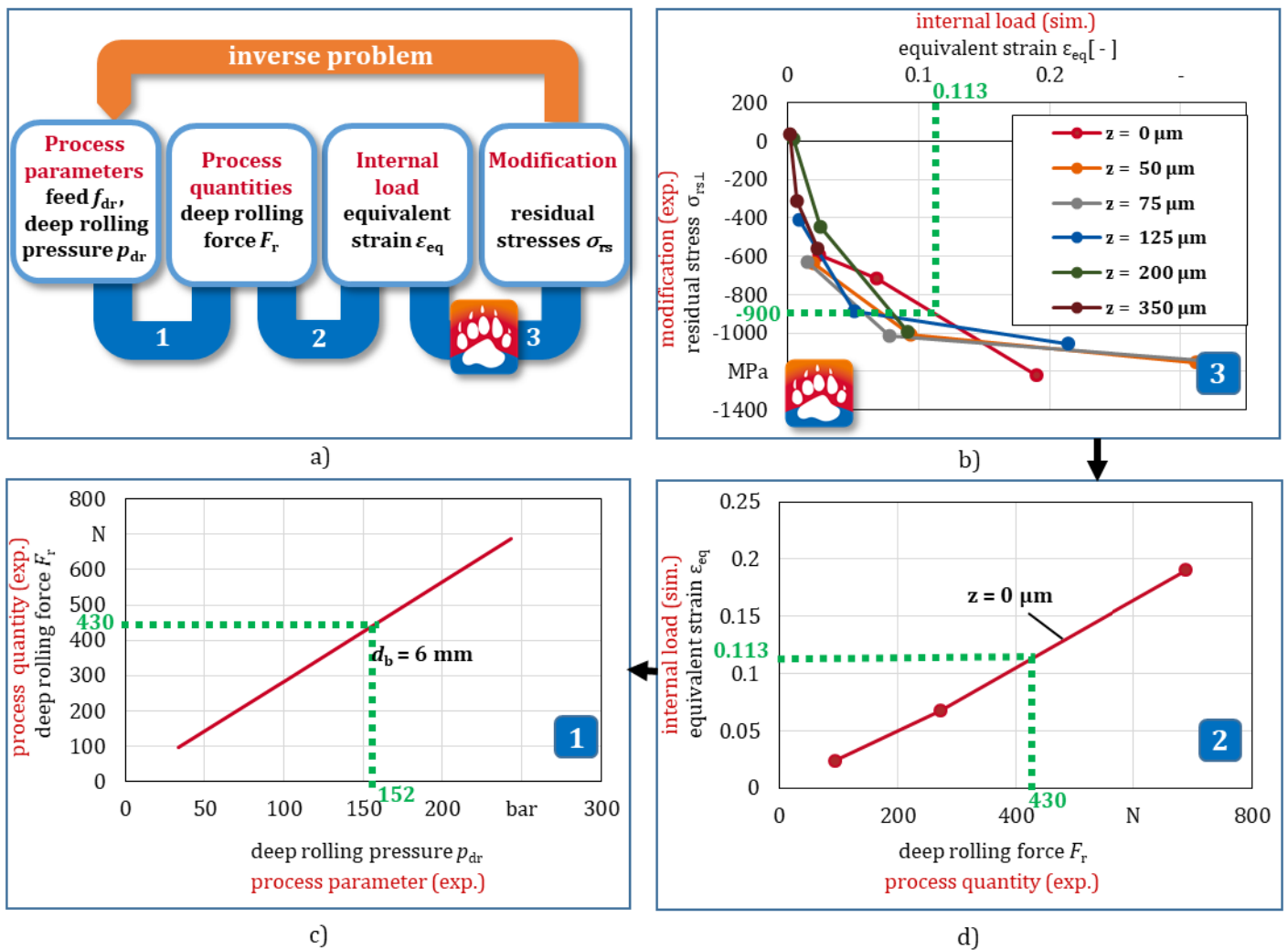


Figure 14 – Procedure to determine the necessary process parameters from a wanted modification of the surface integrity with the help of correlations along the causal sequence of deep rolling.

Acknowledgments

The authors thank the German Research Foundation (DFG) for funding this work within the transregional Collaborative Research Centre SFB/TRR 136 “Process Signatures” - project number 223500200 - subproject M01 and subproject F01. Furthermore, XRD measurements by Heiner Meyer are appreciated.

7. References

- [1] Bleicher, F., Lechner, C., Habersohn, C., Obermair, M., Heindl, F., Rodriguez Ripoll, M.: Improving the tribological characteristics of tool and mould surfaces by machine hammer peening. *CIRP Annals* 2013, 62/1:239-242. DOI: 10.1016/j.cirp.2013.03.043
- [2] Rotella, G., Filice, L., Micari, F.: Improving surface integrity of additively manufactured GP1 stainless steel by roller burnishing. *CIRP Annals* 2020, 69/1:513-516. DOI: 10.1016/j.cirp.2020.04.015
- [3] Yen, Y.C., Sartkulvanich, P., Allen, T.: Finite Element Modeling of Roller Burnishing Process, *CIRP Annals* 2005, 54/1:237-240. DOI: 10.1016/s0007-8506(07)60092-4
- [4] Meyer, D., Wielki, N.: Internal reinforced domains by intermediate deep rolling in additive manufacturing. *CIRP Annals* 2019, 86/1:579-582. DOI: 10.1016/j.cirp.2019.04.012

- [5] Jawahir, I.S., Brinksmeier, E., M'Saoubi, R., Aspinwall, D.K., Outeiro, J.C., Meyer, D., Umbrello, D., Jayal, A.D.: Surface integrity in material removal processes: Recent advances. *CIRP Annals* 2011, 60/2:603-626. DOI: 10.1016/j.cirp.2011.05.002
- [6] Schulze, V., Bleicher, F., Groche, P., Guo, Y.B., Pyun, Y.S.: Surface modification by machine hammer peening and burnishing. *CIRP Annals* 2016, 65/2:809-832. DOI: 10.1016/j.cirp.2016.05.005
- [7] Prabhu, P.R., Kulkarni, S.M., Sharma, S.: Multi-response optimization of the turn-assisted deep cold rolling process parameters for enhanced surface characteristics and residual stress of AISI4140 steel shafts. *Journal of Materials Research and Technology* 2020, 9/5:11402-11423. DOI: 10.1016/j.jmrt.2020.08.025
- [8] Denkena, B., Grove, T., Breidenstein, B., Abrao, A., Meyer, K.: Correlation between process load and deep rolling induced residual stress profiles. *Procedia CIRP* 2018, 78:161-165. DOI: 10.1016/j.procir.2018.09.063
- [9] Delgado, P., Cuesta, I.L., Alegre, J.M., Diaz, A.: State of the art of Deep Rolling. *Precision Engineering* 2016, 46:1-10. DOI: 10.1016/j.precisioneng.2016.05.001
- [10] Brinksmeier, E., Meyer, D., Heinzl, C., Lübben, T., Sölter, J., Langenhorst, L., Frerichs, F., Kämmler, J., Kohls, E., Kuschel, E.: Process Signatures - The Missing Link to Predict Surface Integrity in Machining. *Procedia CIRP* 2018, 71:3-10. DOI: 10.1016/j.procir.2018.05.006
- [11] Meyer, D., Kämmler, J.: Surface Integrity of AISI 4140 After Deep Rolling with Varied External and Internal Loads. *Procedia CIRP* 2016, 45:363-366. DOI: 10.1016/j.procir.2016.02.356
- [12] Kämmler, J., Wielki, N., Meyer, D.: Surface integrity after internal load oriented multistage contact deep rolling. *Procedia CIRP* 2018, 71:490-495. DOI: 10.1016/j.procir.2018.05.026
- [13] Kinner-Becker, T., Sölter, J., Karpuschewski, B.: A simulation-based analysis of internal material loads and material modifications in multi-step deep rolling. *Procedia CIRP* 2020, 87:515-520. DOI: 10.1016/j.procir.2020.02.060
- [14] Brinksmeier, E., Reese, S., Klink, A., Langenhorst, L., Lübben, T.: Underlying Mechanisms for Developing Process Signatures in Manufacturing. *Nanomanuf Metrol* 2018. 1/4:193-208. DOI: 10.1007/s41871-018-0021-z
- [15] Grzesik, W. Application of process signature concept to prediction of the functional properties of machine parts. *Mechanik* 2019, 92/3:158-162. DOI: 10.17814/mechanik.2019.3.25
- [16] Emde, T.: (2009): *Mechanisches Verhalten metallischer Werkstoffe über weite Bereiche der Dehnung, der Dehnrates und der Temperatur*. Aachen, Dr.-Ing. Dissertation RWTH Aachen. 2008.
- [17] Garbrecht, M. *Mechanisches Randschichthärten in der Fertigung*. Bremen: Dr.-Ing. Dissertation Uni Bremen. 2006.
- [18] Chaboche, J. L.: On some modifications of kinematic hardening to improve the description of ratchetting effects. In: *International Journal of Plasticity* 1991. 7/7:661-678. DOI:10.1016/0749-6419(91)90050-9
- [19] Fischer A., Scholtes B., Niendorf T.: Influence of Deep Rolling and Induction Hardening on Microstructure Evolution of Crankshaft Sections made from 38MnSiVS5 and 42CrMo4. *HTM Journal of Heat Treatment and Materials* 2021, 76/3:175-194. DOI: 10.1515/htm-2021-0002